Molecular Dynamics Simulations of Nitrate Complexes with Polyammonium Macrocycles: Insight on Phosphoryl Transfer Catalysis

Garegin Papoyan, Kun-jian Gu, Joanna Wiorkiewicz-Kuczera, Krzysztof Kuczera,* and Kristin Bowman-James*

Contribution from the Departments of Chemistry and Biochemistry, University of Kansas, Lawrence, Kansas 66045

Received January 6, 1995[⊗]

Abstract: Nitrate complexes of two different polyammonium macrocycles, the tetrahydrogen nitrate salts of 1,4,7,-16,19,21-hexaaza-10,13-dioxacyclotetracosane [24]N_6O_2·4HNO_3, **1**, and 1,4,10,13-tetraaza-7,16-dioxacyclooctadecane, [18]N_4O_2·4HNO_3, **2**, have been isolated and their structures determined by X-ray crystallographic methods. Compound **1** crystallizes in the orthorhombic space group *Imma* with unit cell dimensions $a = 22.692(3)$ Å, $b = 19.563(3)$ Å, $c = 7.005(1)$ Å, $V = 3110(1)$ Å^3, and $Z = 4$. Compound **2** crystallizes in the orthorhombic space group *Pbca* with $a = 13.877(1)$ Å, $b = 15.553(1)$ Å, $c = 10.742(1)$ Å, $V = 2314.6(5)$ Å^3, and $Z = 8$. Full-matrix least-squares refinement resulted in $R = 0.051$ and $R_w = 0.067$ for **1** and $R = 0.063$ and $R_w = 0.072$ for **2**. Compound **1** has a boat-shaped geometry, and one of the four nitrates is situated in the macrocyclic cavity. Compound **2** is relatively flat with two nitrates above and two below the plane of the molecule. Molecular dynamics simulations were performed for the two molecules using the structural coordinates obtained from the crystal structures and the CHARMM molecular model. Simulations were carried out to 400 ps for **1** and 200 ps for **2** using 2 fs time steps. The average temperature during the simulation was 302 ± 5 K and the average total energy was -7805.9 ± 0.5 kcal mol^{-1} for **1** and -7851.9 ± 0.5 kcal mol^{-1} for **2**. The conformation of **2** did not change appreciably during the simulations, whereas **1** flattened out considerably due to hydration effects.

Introduction

Although analytical chemists have utilized the concept of anion recognition for many years, the field entered the "supramolecular" era in 1968. At that time Park and Simmons reported that simple diaza bicyclic catapinands form inclusion complexes in which halides are incorporated within the bicycle.[1] The use of macrocyclic receptors for anion recognition slowly began to grow in the 1970s, with findings that these molecules could recognize a multitude of anionic species: simple inorganic ions such as nitrates, perchlorates, sulfates, and azide; more complex molecules such as dicarboxylic acids and polyphosphates; and ultimately anionic metal ion complexes.[2] The binding sites for anion complexation are usually, although not always, ammonium ions, and much of the stabilization results from strong $^+$N−H···X$^-$ hydrogen bonds and electrostatic interactions between positively charged macrocycles and negatively charged anions.

In the early 1980s the discovery that a simple monocyclic macrocycle, 1,4,7,16,19,21-hexaaza-10,13-dioxacyclotetracosane [24]N_6O_2, **1**,[3] formed high-affinity complexes with nucleotides and also catalyzed their hydrolysis led to exciting new applications of these molecules as protoenzymes for phosphoryl transfer reactions. ATPase,[4] kinase,[5] and N^{10}-formyltetrahydrofolate synthetase[6] activities were reported. Oxygen-labeling studies indicate that a metaphosphate intermediate is likely.[7] Kinetic studies of a number of different polyammonium macrocycles point to the importance of ring size as a crucial factor governing catalytic rates,[8] with maximum catalytic capability achieved for macromonocycles with 21- to 24-membered rings. Early modeling studies in our laboratory suggested that an important consideration may be hydrogen-bonding interactions between the terminal phosphate of ATP and both triamine "sides" of

[⊗] Abstract published in *Advance ACS Abstracts,* January 1, 1996.

(1) Park, C. H.; Simmons, H. E. *J. Am. Chem. Soc.* **1968**, *90*, 2431−2432.

(2) (a) Graf, E.; Lehn, J.-M. *J. Am. Chem. Soc.* **1968**, *90*, 2431−2432. (b) Dietrich, B.; Hosseini, M. W.; Lehn, J.-M.; Sessions, R. B. *J. Am. Chem. Soc.* **1981**, *103*, 1282−1283. (c) Coquhoun, H. M.; Stoddart, J. F.; Williams, D. J. *Angew. Chem., Int. Ed. Engl.* **1986**, *25*, 487−507. (d) Schmidtchen, F. *J. Am. Chem. Soc.* **1986**, *108*, 8249−8255. (e) Reddington, M. V.; Spencer, N.; Stoddart, J. F. In *Inclusion Phenomena and Molecular Recognition*; Atwood, J. L., Ed.; Plenum: New York, 1990; pp 41−48. (f) Breslow, R.; Duggan, P. J.; Wiedenfeld, D.; Waddell, S. T. *Tetrahedron Lett.* **1995**, *36*, 2707−2710. (g) Katz, H. E. In *Inclusion Compounds*; Atwood, J. L., Davies, J. E. D., MacNicol, D. D., Eds.; Oxford University Press: Oxford, 1991; Vol. 4, pp 391−405. (h) Kaufmann, D. E.; Otten, A. *Angew. Chem., Int. Ed. Engl.* **1994**, *33*, 1832−1834. (i) Bianchi, A.; Micheloni, M.; Paoletti, P. *Coord. Chem. Rev.* **1991**, *110*, 17−113. (j) Dietrich, B.; Guilhem, J.; Lehn, J.-M.; Pascard, C.; Sonveaux, E. *Helv. Chim. Acta* **1984**, *67*, 91−104. (k) Cullinane, J.; Gelb, R. I.; Margulis, T. N.; Zompa, L. J. *J. Am. Chem. Soc.* **1982**, *104*, 3045−3053.

(3) Hosseini, M. W.; Lehn, J.-M.; Mertes, M. P. *Helv. Chim. Acta* **1983**, *66*, 2454−2466.

(4) (a) Hosseini, M. W.; Lehn, J.-M. *Helv. Chim. Acta* **1985**, *68*, 818. (b) Hosseini, M. W.; Lehn, J.-M.; Maggiora, L.; Mertes, K. B.; Mertes, M. P. *J. Am. Chem. Soc.* **1987**, *109*, 537−544. (c) Hosseini, M. W.; Lehn, J.-M.; Jones, K. C.; Plute, K. E.; Mertes, K. B.; Mertes, M. P. *J. Am. Chem. Soc.* **1989**, *111*, 6330−6335.

(5) (a) Hosseini, M. W.; Lehn, J.-M. *J. Chem. Soc., Chem. Commun.* **1985**, 1155−1157. (b) Yohannes, P. G.; Mertes, M. P.; Mertes, K. B. *J. Am. Chem. Soc.* **1985**, *107*, 8288−8289. (c) Hosseini, M. W.; Lehn, J.-M. *J. Am. Chem. Soc.* **1987**, *109*, 7046−7058. (d) Yohannes, P. G.; Plute, K. E.; Mertes, M. P.; Mertes, K. B. *Inorg. Chem.* **1987**, *26*, 1751−1755. (e) Hosseini, M. W.; Lehn, J.-M. *J. Chem. Soc., Chem. Commun.* **1988**, 397−399.

(6) (a) Jiang, Z.; Chalabi, P.; Mertes, K. B.; Jahansouz, H.; Himes, R. H.; Mertes, M. P. *Bioorg. Chem.* **1989**, *17*, 313−319. (b) Jahansouz, H.; Jiang, Z.; Himes, R. H.; Mertes, M. P.; Mertes, K. B. *J. Am. Chem. Soc.* **1989**, *111*, 1409−1413.

(7) (a) Bethell, R. C.; Lowe, G.; Hosseini, M. W.; Lehn, J.-M. *Bioorg. Chem.* **1988**, *16*, 418−428. (b) Blackburn, G.; Thatcher, G. R. J.; Hosseini, M. W.; Lehn, J.-M. *Tetrahedron Lett.* **1987**, *28*, 2779−2782.

(8) (a) Qian, L.; Sun, Z.; Gao, J.; Movassagh, B.; Morales, L.; Mertes, K. B. *J. Coord. Chem.* **1991**, *23*, 155−172. (b) Bencini, A.; Bianchi, A.; Garcia-Espana, E.; Scott, E. C.; Morales, L.; Wang, B.; Mertes, M. P.; Mertes, K. B. *Bioorg. Chem.* **1992**, *20*, 8−29.

the macrocycle.[9] While single crystals suitable for X-ray analysis of **1** with nucleotides or other phosphate species have not been obtained, we have recently isolated crystals of the nitrate complex (interestingly, an analog of metaphosphate) of the tetraprotonated form of **1**, as well as the nitrate complex of the related 18-membered ring system, 1,4,10,13-tetraaza-7,16-dioxacyclooctadecane, [18]N$_4$O$_2$, **2**.
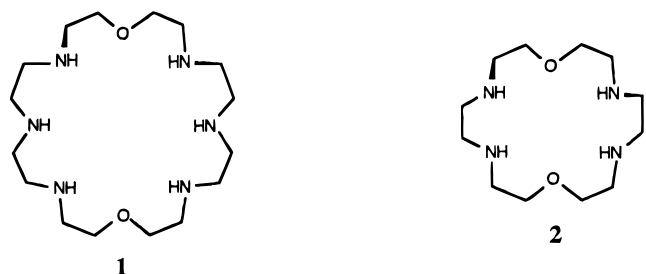
Because of our interest in bridging from solid state to solution structural influences, and in understanding consequences of solvation on reaction pathways, we chose to examine the structural relationships between the macrocyclic cation and nitrate anion in solution by molecular dynamics (MD) simulations. MD simulations have emerged as an important tool in the study of molecular motion in physics, chemistry, and biology.[10,11] Within the adopted molecular model, molecular dynamics trajectories contain complete classical descriptions of simulated systems on the atomic level of detail, yielding time scales, amplitudes, and energetics of atomic motions in the system. Trajectories can be used to investigate both time-dependent phenomena, as in conformational transitions, and thermodynamic averages.[10] In recent years, due to the development of new and more efficient algorithms and increases in available computer power, realistic simulations of chemically and biologically important molecules, involving both explicit inclusion of solvent and realistic boundary conditions to compensate for the finite size of the system, have become feasible.[10,12]

The use of molecular dynamics simulations has been especially informative for macrocyclic systems where preorganization plays such a major role. Hence, simulations have been performed for crown ethers,[13,14] thia crown ethers,[15] cryptands,[13] and cavitands[16] as receptors for cations. Far fewer investigations have been reported for the interactions of macrocyclic hosts with anionic guests, however. In earlier works the interactions of chloride and bromide ion with the spherical bicyclic "soccer ball" ligand[17] and chloride interaction with two other monocyclic aza macrocycles including **1**[18] were examined. These previous studies were only performed with simple monatomic halide ions,

Table 1. Crystallographic Data for [24]N$_6$O$_2$·4HNO$_3$ (**1**·4HNO$_3$) and [18]N$_4$O$_2$·4NO$_3$ (**2**·4HNO$_3$)

	1·4HNO$_3$	**2**·4HNO$_3$
formula	C$_{16}$H$_{42}$N$_{10}$O$_{14}$	C$_{12}$H$_{32}$N$_8$O$_{14}$
fw	598.57	512.44
crystal color, habit	colorless, plate	colorless, prism
crystal dimensions, mm	0.4 × 0.2 × 0.1	0.3 × 0.2 × 0.1
crystal system	orthorhombic	orthorhombic
space group	*Imma* (no. 74)	*Pbca* (no. 61)
a (Å)	22.692(3)	13.877(1)
b (Å)	19.563(3)	15.553(1)
c (Å)	7.005(1)	10.724(1)
V (Å^3)	3110(1)	2314.6(5)
Z	4	8
ρ_{calc}, g/cm	1.278	1.470
diffractometer	Rigaku AFC5R	Rigaku AFC5R
temp, °C	23	23
radiatn wavelength (Å)	1.541 78 (Cu Kα)	1.541 78 (Cu Kα)
μ, cm^{-1}	11.17	9.18
scan method	$\omega - 2\theta$	$\omega - 2\theta$
scan rate (deg/min in ω)	2.0	32.0
2θ max, deg	112.6	112.6
no. reflecns collected	1781	1201
observation criterion	$I > 0.01\sigma(I)$	$I > 3.0\sigma(I)$
no. observed reflecns	1398	912
no. variables	218	155
reflecn/parameter	6.41	5.88
final R	0.051	0.063
final R_w	0.067	0.072
goodness of fit	0.99	1.18

however. Here we report the results of the crystal structures of [24]N$_6$O$_2$·4HNO$_3$ (**1**·4HNO$_3$) and [18]N$_4$O$_2$·4HNO$_3$ (**2**·4HNO$_3$) and the results of the first extended molecular dynamics simulations of more complex anionic guests, the solution interactions of the two macrocycles with nitrate ion. The results of these studies show that ring size can have a major influence on the conformation and ionic interactions in solution and that solvation plays a major role in cation−anion interactions.

Experimental Section

Synthesis. The syntheses of the two macrocycles, **1** and **2**, were carried out as previously described.[3,19] Crystals of the nitrate complex of **1** suitable for X-ray determination were obtained by reacting uranyl nitrate (0.52 g, 1.04 mmol) in 10 mL of CH$_3$OH with the free base of **1** (0.36 g, 1.04 mmol) in 15 mL of CH$_2$Cl$_2$. Colorless crystals precipitated within 2 days after initial precipitation of uranyl salts. Crystals of the nitrate complex of **2** were prepared in a similar manner.

X-ray Data Collection. Crystallographic data for **1**·4HNO$_3$ and **2**·4HNO$_3$ are summarized in Table 1; atomic coordinates, selected interatomic distances and angles, and dihedral angles for **1**·4HNO$_3$ are in Tables 2, 3, and 4, respectively, for **1**·4HNO$_3$, and in Tables 5, 6, and 7, respectively, for **2**·4HNO$_3$. All measurements were made on a Rigaku AFC5R diffractometer with graphite monochromated Cu Kα radiation and a 12 kW rotating anode generator. Cell constants and an orientation matrix for data collection were obtained from a least-squares refinement using the setting angles of 25 carefully centered reflections for **1** and 12 reflections for **2**. The data were collected at a temperature of 23 ± 1 °C using the $\omega - 2\theta$ scan technique to a maximum 2θ value of 112.6°. The weak reflections ($I < 10.0\sigma(I)$) were rescanned (maximum of two rescans), and the counts were accumulated to assure good counting statistics. Stationary background counts were recorded on each side of the reflection. The ratio of peak counting time to background counting time was 2:1. The diameter of

(9) Mertes, M. P.; Mertes, K. B. *Acc. Chem. Res.* **1990**, *23*, 413−418.

(10) Brooks, C. L., III; Karplus, M.; Petitt, B. M. In *Proteins: A Theoretical Perspective of Dynamics, Structure, and Thermodynamics*; John Wiley and Sons: New York, 1988.

(11) van Gunsteren, W. F.; Berendsen, H. J. C. *Angew. Chem., Int. Ed. Engl.* **1990**, *29*, 992−1023.

(12) Tobias, D. J.; Mertz, J. E.; Brooks, C. L., III. *Biochemistry* **1991**, *30*, 6054−6058.

(13) (a) Rangino, G.; Romano, M. S.; Lehn, J.-M.; Wipff, G. *J. Am. Chem. Soc.* **1985**, *107*, 7873−7877. (b) Straatsma, T. P.; McCammon, J. A. *J. Chem. Phys.* **1989**, *91*, 3631−3637. (c) Cieplak, P.; Kollman, P. J. *Phys. Chem.* **1990**, *92*, 6761−6767. (d) Liem, S. D.; Kollman, P. A. *J. Phys. Chem.* **1995**, *99*, 55−58. (f) Ha, Y. L.; Chakraborty, A. K. *J. Phys. Chem.* **1991**, *95*, 10781.

(14) Troxler, L.; Wipff, G. *J. Am. Chem. Soc.* **1994**, *116*, 1468−1480.

(15) Forsyth, G. A.; Lockhart, J. C. *J. Chem. Soc., Dalton Trans.* **1994** 697−703.

(16) (a) Bayly, C. I.; Kollman, P. A. *J. Am. Chem. Soc.* **1994**, *116*, 697−703. (b) Thomas, B. E, IV; Kollman, P. A. *J. Am. Chem. Soc.* **1994**, *116*, 3449−3452.

(17) (a) Lybrand, T. P.; McCammon, J. A.; Wipff, G. *Proc. Natl. Acad. Sci. U.S.A.* **1986**, *83*, 833−835. (b) Owenson, B.; MacElroy, R. D.; Pohorille, A. *J. Am. Chem. Soc.* **1988**, *110*, 6992−7000. (c) Owenson, B.; MacElroy, R. D.; Pohorille, A. *THEOCHEM* **1988**, *179*, 467−484.

(18) Boudon, S.; Decian, A.; Fischer, J.; Hosseini, M. W.; Lehn, J.-M.; Wipff, G. *J. Coord. Chem.* **1991**, *23*, 113−135.

(19) Biernat, J. F.; Luboch, E. *Tetrahedron* **1984**, *49*, 110.

Table 2. Atomic Coordinates ($\times 10^4$ Å) and Isotropic Thermal Parameters for $[24]N_6O_2 \cdot 4HNO_3$ (**1·4HNO₃**)

atom	x	y	z	B(eq)
N(1)	3443(2)	2500	232(5)	3.5(2)
C(2)	3541(2)	3136(2)	−825(5)	4.2(2)
C(3)	3534(2)	3717(2)	515(5)	4.2(2)
N(4)	4003(1)	3631(2)	2017(4)	3.6(1)
C(5)	3974(2)	4115(2)	3625(6)	4.2(2)
C(6)	4481(2)	3995(2)	4952(6)	4.4(2)
O(7)	5000	4170(1)	3987(4)	3.9(2)
N(1A)	5000	2500	63(2)	7.2(5)
O(1A)	5000	2500	211(2)	7.0(4)
O(2A)	5000	3080(4)	−32(1)	10.0(4)
N(1B)	3152(2)	2500	4604(5)	3.8(2)
O(1B)	2888(1)	3049(1)	4603(4)	5.2(1)
O(2B)	3711(1)	2500	4571(4)	4.1(2)
N(1C)	5000	5000	0000	5.4(4)
O(1C)	5480(3)	5199(3)	27(1)	6.0(4)
O(2C)	5000	4269(4)	−29(1)	5.2(4)

Table 3. Atomic Coordinates ($\times 10^4$ Å) and Isotropic Thermal Parameters for $[18]N_4O_2 \cdot 4HNO_3$ (**2·4HNO₃**)

atom	x	y	z	B(eq)
N(1)	9849(2)	1340(2)	−1552(3)	3.5(1)
C(2)	9446(3)	2205(2)	−1270(4)	4.3(1)
C(3)	8517(3)	2120(2)	−571(3)	4.2(1)
O(4)	8717(1)	1694(1)	567(2)	4.3(1)
C(5)	7880(3)	1495(2)	1271(4)	4.5(2)
C(6)	8180(3)	891(2)	2292(3)	4.5(2)
N(7)	8634(2)	105(2)	1766(2)	3.5(1)
C(8)	8925(3)	−514(2)	2746(3)	3.9(1)
C(9)	9212(2)	−1373(3)	2229(4)	4.1(2)
N(1A)	10802(2)	1184(2)	1388(3)	4.3(1)
O(1A)	10497(1)	567(1)	714(2)	3.9(1)
O(2A)	11203(2)	1799(2)	894(3)	6.4(1)
O(3A)	10681(2)	1150(2)	2520(2)	6.3(1)
N(1B)	8470(2)	759(2)	−4108(3)	4.3(1)
O(1B)	7854(2)	449(2)	−4813(2)	6.2(1)
O(2B)	8268(2)	828(2)	−2987(2)	6.3(1)
O(3B)	9264(2)	987(2)	−4498(3)	6.7(1)

Table 4. Selected Bond Lengths (Å) and Angles (deg) for $[24]N_6O_2 \cdot 4HNO_3$ (**1·4HNO₃**)

N(1)−C(2)	1.465(4)	N(4)−C(5)	1.473(5)
C(2)−C(3)	1.474(5)	C(5)−C(6)	1.498(6)
C(3)−N(4)	1.506(5)	C(6)−O(7)	1.403(4)

C(2)−N(1)−C(2′)	116.3(4)	N(4)−C(5)−C(6)	109.9(3)
N(1)−C(2)−C(3)	109.4(3)	C(5)−C(6)−O(7)	107.8(4)
C(2)−C(3)−N(4)	110.5(3)	C(6)−O(7)−C(6′)	114.1(4)
C(3)−N(4)−C(5)	115.5(3)		

Table 5. Selected Bond Lengths (Å) and Angles (deg) for $[24]N_6O_2 \cdot 4HNO_3$ (**2·4HNO₃**)

N(1)−C(2)	1.489(4)	C(5)−C(6)	1.502(5)
C(2)−C(3)	1.497(5)	C(6)−N(7)	1.488(4)
C(3)−O(4)	1.416(4)	N(7)−C(8)	1.481(4)
O(4)−C(5)	1.419(4)	C(8)−C(9)	1.499(4)

C(2)−N(1)−C(9)	113.3(2)	C(5)−C(6)−N(7)	110.8(3)
N(1)−C(2)−C(3)	110.1(3)	C(6)−N(7)−C(8)	112.4(2)
C(2)−C(3)−O(4)	107.7(3)	N(7)−C(8)−C(9)	112.9(3)
C(3)−O(4)−C(5)	113.6(2)	C(8)−C(9)−N(1)	112.4(3)
O(4)−C(5)−C(6)	107.3(3)		

the incident beam collimator was 0.5 mm, and the crystal to detector distance was 285.0 mm.

The intensities of three representative reflections, measured after every 150 reflections, remained constant throughout data collection indicating crystal and electronic stability. No decay correction was applied. An empirical absorption correction was applied using the program DIFABS.[20] The data were corrected for Lorentz and polarization effects. No extinction corrections were applied.

Table 6. Dihedral Angles (deg) for $[24]N_6O_2 \cdot 4HNO_3$ (**1·4HNO₃**)

atoms	angle	atoms	angle
C(2′)−N(1)−C(2)−C(3)	169.4(3)	C(3)−N(4)−C(5)−C(6)	−177.1(3)
N(1)−C(2)−C(3)−N(4)	58.6(4)	N(4)−C(5)−C(6)−O(7)	66.5(4)
C(2)−C(3)−N(4)−C(5)	−169.9(3)	C(5)−C(6)−O(7)−C(6′)	−171.2(2)

Table 7. Dihedral Angles (deg) for $[18]N_4O_2 \cdot 4HNO_3$ (**2·4HNO₃**)

atoms	angle	atoms	angle
N(1)−C(2)−C(3)−O(4)	61.5(4)	C(6)−N(7)−C(8)−C(9)	169.3(3)
C(2)−C(3)−O(4)−C(5)	−174.2(3)	C(3)−C(2)−N(1)−C(9)	−178.9(3)
C(3)−O(4)−C(5)−C(6)	168.2(3)	C(2)−N(1)−C(9)−C(8)	−167.6(3)
O(4)−C(5)−C(6)−N(7)	−57.9(4)	N(1)−C(9)−C(8)−N(7)	−71.0(4)
C(5)−C(6)−N(7)−C(8)	−179.0(3)		

Structure Solution and Refinement. The structure was solved by direct methods.[21] Refinement was performed using full-matrix least-squares methods. The non-hydrogen atoms were refined anisotropically. Hydrogen atom positions were located from a difference map after all the non-hydrogens were located. The weighting scheme was based on counting statistics and included a factor ($p = 0.05$) to downweight the intense reflections. Neutral atom scattering factors were taken from Cromer and Waber.[22] Anomalous dispersion effects were included in F_{calc}.[23] All calculations were performed using the TEXSAN crystallographic software package of the Molecular Structure Corp.[24]

Details of the Force Field Parameterization. In order to create force field parameters for the macrocycle, three new atoms were introduced in CHARMM: OS3, an ether oxygen; NS3, a secondary amine nitrogen; and NS4, a secondary ammonium cation nitrogen. Initial parameters except parameters for carbon and hydrogen were transferred from SYBYL[25] to the CHARMM force field and were altered to fit *ab initio* HF/6-31+G* [26] vibrational frequencies of diethyl ether, diethylamine, and diethylammonium cation, respectively. All parameters are shown in Table 8. The nitrate ion was introduced in the same way by new atoms: NO as a nitrogen and ON as an oxygen in the nitrate anion. Parameters were created to fit *ab initio* vibrational frequencies of nitrate anion calculated on the NMP2/6-31G* theoretical level. The nitrate anion was calculated with D_{3h} symmetry, diethylamine with C_s symmetry, and diethylammonium cation and diethyl ether with C_{2v} symmetry. All *ab initio* frequencies were scaled by 0.9 to correct for systematic errors.

RMS deviations between vibrational frequencies calculated in CHARMM with new parameters and theoretical *ab initio* frequencies are 11.8 cm^{-1} for the nitrate anion, 45.4 cm^{-1} for diethyl ether, 41.4 cm^{-1} for diethylamine, and 47.4 cm^{-1} for diethylammonium cation. The somewhat high rms deviations for the diethyl ether, diethylamine, and diethylammonium cation are a result of using unaltered parameters for carbon and hydrogen from the CHARMM force field. The rms deviations for vibrations which did not include CH₂ are much lower. These should be sufficient in "chemical accuracy" for the nonspectroscopic purposes here,[27] although spectroscopists are frequently interested in accuracy on the order of 3 cm^{-1} (0.009 kcal/mol).

Charges for all atoms were estimated by the CHELP charge fitting technique in the Gaussian-92[26] package on MP2/6-31G theoretical level

(20) Walker, N.; Stuart, D. *Acta Cerystallogr.* **1983**, *A39*, 158−166.

(21) (a) Gilmore, C. J. *J. Appl. Crystallogr.* **1984**, *17*, 42−46. (b) Beurskens, P. T. Technical Report Crystallography Laboratory, Toernooiveld, 6525 E. Nijmegen, Netherlands, 1985.

(22) Cromer, D. T.; Waber, J. T. In *International Tables for X-ray Crystallography*; Kynoch Press: Birmingham, 1974; Vol. IV, Tables 2.2A and 2.3.1.

(23) Ibers, J. A.; Hamilton, W. C. *Acta Crystallogr.* **1964**, *17*, 781.

(24) TEXSAN-TEXRAY Structure Analysis Package, Molecular Structure Corp., 1985.

(25) Matthew, C.; Cramer, R. D.; van Opdenbosh, N. *J. Comput. Chem.* **1989**, *10*, 6761−6767.

(26) Frisch, M. J.; Trucks, W.; Head-Gordon, M.; Gill, P. M. W.; Wong, M. W.; Foresman, J. B.; Johnson, B. G.; Schlegel, H. B.; Robb, M. A.; Replogle, E. S.; Gomperts, R.; Andres, J. L.; Raghavachari, K.; Binkley, J. S.; Gonzales, C.; Martin, R. L.; Fox, D. J.; Defrees, D. J.; Baker, J.; Stewart, J. J. P.; Pople, J. A. *Gausian 92, Revision C*; Gaussian, Inc.: Pittsburgh, PA, 1992.

(27) Allinger, N. L.; Yuh, Y. H.; Lii, J.-H. *J. Am. Chem. Soc.* **1989**, *111*, 8852−8858.

Table 8. Force Field Parameters

a) Bond stretching parameters

Bond		$K_R(\frac{kcal}{mol*A^2})$	$R(Å)$
NO	ON	400.00	1.273
CT2	OS3	265.00	1.400
CT2	NS3	365.00	1.450
CT2	NS4	340.00	1.470
NS3	H	440.00	1.090
NS4	H	425.00	1.080
NO	ON	400.00	1.273

b) VDW parameters

Atom	$K(\frac{kcal}{mol})$	$R(Å)$
NO	-0.141000	2.080000
ON	-0.223000	1.840000
NS3	-0.095000	1.550000
NS4	-0.095000	1.550000
OS3	-0.116000	1.520000

c) Torsional parameters in terms of Fourier series

Torsional angle				$V_0(\frac{kcal}{mol})$	n
H	NS4	CT2	HA	0.1300	3
CT2	NS4	CT2	HA	0.1300	3
H	NS3	CT2	HA	0.1500	3
CT2	NS3	CT2	HA	0.1500	3
CT2	NS3	CT2	CT2	0.1500	3
CT2	NS4	CT2	CT2	0.1300	3
H	NS3	CT2	CT2	0.1500	3
H	NS4	CT2	CT2	0.1300	3
NS3	CT2	CT2	HA	0.2000	3
NS4	CT2	CT2	HA	0.2000	3
NS4	CT2	CT2	NS3	0.3200	3
OS3	CT2	CT2	HA	0.2700	3
OS3	CT2	CT2	NS3	0.3200	3
OS3	CT2	CT2	NS4	0.3200	3
CT2	OS3	CT2	CT2	0.1900	3
CT2	OS3	CT2	HA	0.1800	3
Improper torsional deformation					
NO	X	X	ON	100.0	

d) Angle bending parameters

	Angle		$K_\theta(\frac{kcal}{mol*rad^2})$	$\theta_0(deg)$	$K_{UB}(\frac{kcal}{mol*A^2})$	$R_{UB}(Å)$
ON	NO	ON	62.0	120.0	75.0	2.21
OS3	CT2	CT2	55.0	109.5	5.00	2.36
OS3	CT2	HA	53.0	109.5	12.00	2.05
CT2	OS3	CT2	80.0	109.5	20.0	2.10
CT2	NS3	CT2	80.0	109.5	20.0	2.10
NS3	CT2	CT2	54.0	109.5	—	—
NS3	CT2	HA	47.0	109.5	15.00	2.10
CT2	NS4	CT2	71.5	109.5	—	—
NS4	CT2	CT2	47.0	109.5	—	—
NS4	CT2	HA	47.0	109.5	5.00	2.10
H	NS4	CT2	48.0	109.5	12.00	2.04
H	NS4	H	48.1	109.5	—	—
H	NS3	CT2	31.5	109.5	11.00	2.04
ON	NO	ON	62.0	120.0	75.0	2.205

e) Charges

Group NO_3^-	
Atom ON	0.29
Atom NO	-0.43
Group CH_2	
Atom CT2	0.02
Atom HA	0.09
Group NH	
Atom NS3	-0.70
Atom H	0.30
Group NH_2^+	
Atom NS4	-0.30
Atom H	0.45
Group O	
Atom OS3	-0.70

for nitrate and HF/6-31+G level for others (Table 8d). Charges for all groups of atoms are shown in Table 8e. Lennard-Jones parameters for the new atom types were transferred from chemically related atom types existing in CHARMM.

Molecular Dynamics Simulation Protocol. The initial geometries of the $[24]N_6O_2 \cdot 4HNO_3$ (**1**·4HNO₃) and $[18]N_4O_2 \cdot 4HNO_3$ (**2**·4HNO₃) were taken from the X-ray structure data. For **1**·4HNO₃ only one of the disordered nitrates was chosen for the simulation to allow for the correct charge. The macrocycles were placed in a preequilibrated truncated octahedral water cell, based on a cube of edge 37.86 Å and containing 906 TIP3P model water molecules. After deletion of water overlapping the solute, the system contained 882 water molecules. In Molecular Dynamics simulations SHAKE[28] constraints were imposed on bonds involving hydrogen atoms allowing use of a 2 fs time step. In energy calculations a 12.0 Å nonbonded cutoff distance was employed, with a switching function between 10.0 and 12.0 Å for van der Waals terms and a shift function at 12.0 Å for electrostatics, in order to eliminate discontinuities due to the cutoff.[29] The new amended CHARMM molecular model was used.[30] Full nonbonded interactions were calculated for all atoms separated by three or more chemical bonds.

The system was prepared by energy minimization, 10 ps of heating by random velocity assignments at stepwise increasing temperatures, and 10 ps equilibration at 300 K. Starting from the final structure of this equilibration a 400 ps molecular dynamics simulation was performed for **1** and a 200 ps simulation for **2**. The Verlet algorithm was used for integration of equations of motion in all simulations. Periodic boundary conditions were applied, and the simulation conditions corresponded to the NVE ensemble. The average temperature for both **1** and **2** during the simulation was 302 ± 5 K and the average total energy was −7805.9 ± 0.5 kcal mol⁻¹ for **1** and −7851.9 ± 0.5 kcal mol⁻¹ for **2**.

Results and Discussion

Crystal Structures: Structure of 1·4HNO₃. The results of the crystal structure are shown in the perspective drawings in Figure 1. View A indicates the relationship of the nitrates to the macrocyclic cavity. The nitrates exhibit *mm* symmetry disorder, so the view shown is one of the average representative orientations. The presence of the disorder does not detract from

(28) Ryckaert, J. P.; Gicotti, G.; Berendson, H. J. C. *J. Comput. Chem.* **1977**, *23*, 327−341.

(29) (a) Brooks, J. P.; Bruccoleri, R.; Olafson, B.; States, D.; Swaminathan, S.; Karplus, M. *J. Comput. Chem.* **1983**, *4*, 187−217.
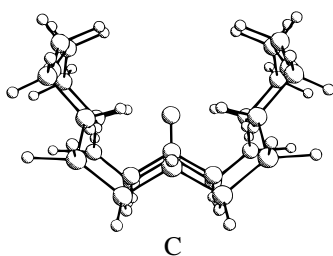
(30) (a) MacKerell, A. D., Jr.; Field, M.; Fischer, S.; Watanabe, M.; Karplus, M. Manuscript in preparation. (b) Kaminski, G.; Duffy, E. M.; Matsui, T.; Jorgensen, W. L. *J. Phys. Chem.* **1994**, *98*, 13077−13082.

Scheme 1. Reaction of **1** with ATP[a]
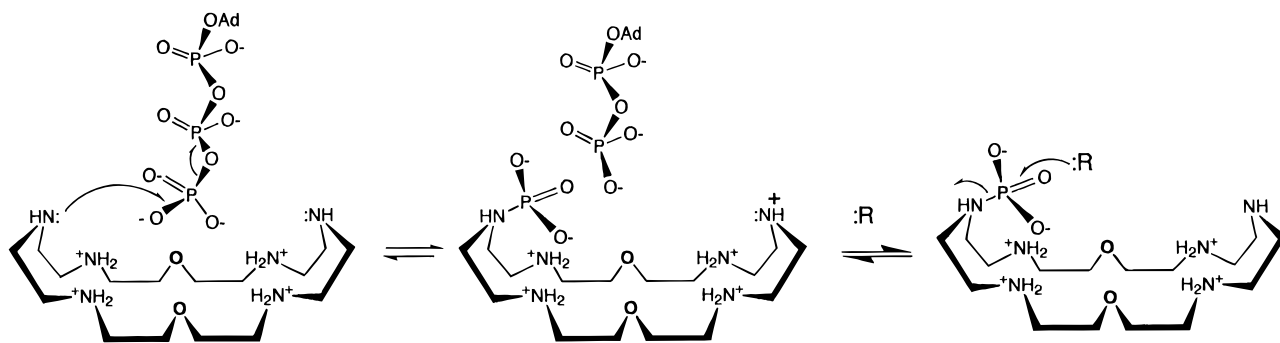
[a] R represents a nucleophile.
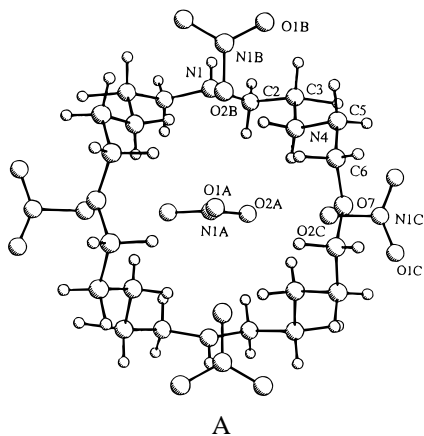
A
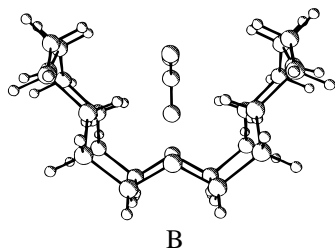
B

C

Figure 1. Overhead (A) and side views (B and C) of the nitrate complex of [24]N$_6$O$_2$, **1**·H4NO$_3$. In (B) and (C) only the encapsulated nitrate is shown for clarity.

the validity of the structure, however, nor the general position of nitrate A. One pair of nitrates (C) has an occupancy of 50%, so the total nitrate count is four: one A; a pair of B; and one-half of each of the pairs C.

The macrocycle, by virtue of its high symmetry, has a very symmetrical pattern of dihedral angles as shown in Table 4. Starting with C(2)−N(1)−C(2)−C(3) as *trans*, N(1)−C(2)−C(3)−N(4) as *gauche*, C(2)−C(3)−N(4)−C(5) and C(3)−N(4)−C(5)−C(6) as *trans*, N(4)−C(5)−C(6)−C(7) as *gauche*, and C(5)−C(6)−O(7)−C(6′) as *trans*, the *gauche−trans−trans−gauche−trans−trans* pattern continues around the entire ring. Furthermore, the hydrogen on N(1) is pointing out of the ring, resulting in an *endo* configuration for the macrocycle.
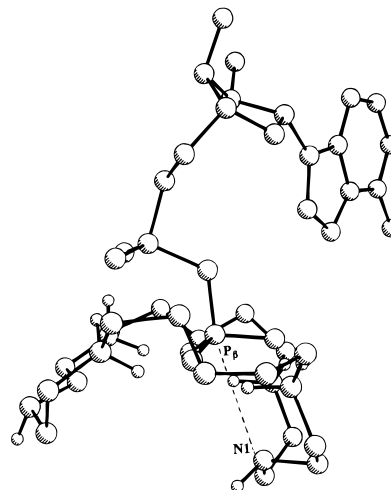

Figure 2. Model study of the docking of ADP into [24]N$_6$O$_2$, **1**. The potential interaction of the amine on the macrocycle with the terminal phosphate is indicated by the dashed line.

Bond distances clearly indicate hydrogen-bonding interactions between the nitrates and the cationic macrocycle. By virtue of the mirror symmetry, the internally "coordinated" nitrate is held in a 4-fold hydrogen-bonding network between O(2A) and N(4) (O(2A)−H(7) = 2.24(5) Å). Nitrate B is held by a 2-fold grip via O(2B)−H(6)−N(4) (O(2B)−H(6) = 2.09(4) Å). The disordered nitrate is only weakly associated with N(4) (O(2C)−H(7) = 2.37(5) Å).

Nitrate ion is an established analog for metaphosphate as illustrated by the crystal structure of the Mn(II)ADP−nitrate lyxose complex in the active site of hexokinase.[31] The nitrate ion in **1**, therefore, ideally represents a metaphosphate analog as previously proposed in the catalytic cycle for dephosphorylation of ATP catalyzed by **1** (Scheme 1).[7] Furthermore, **1** is in the tetraprotonated form in the structure, as found at physiological pH, leaving the two lone pairs on the "central" amines available to nucleophilically attack the terminal phosphate. Views B and C from Figure 1 indicate the ideal positioning of the nitrate with respect to the lone pairs on the central macrocyclic amines with an N(1)−N(1A) distance of 3.54 Å.

These structural results also support previous modeling studies in which ADP was manually docked into the macrocycle, followed by energy minimizations using AMBER and MM2 force fields.[9] In the minimized structure, hydrogen-bonding interactions were observed between both triamine sides of the macrocycle (Figure 2). Extensive hydrogen bonding between macrocycle and substrate has been cited[8,9] as a major factor in

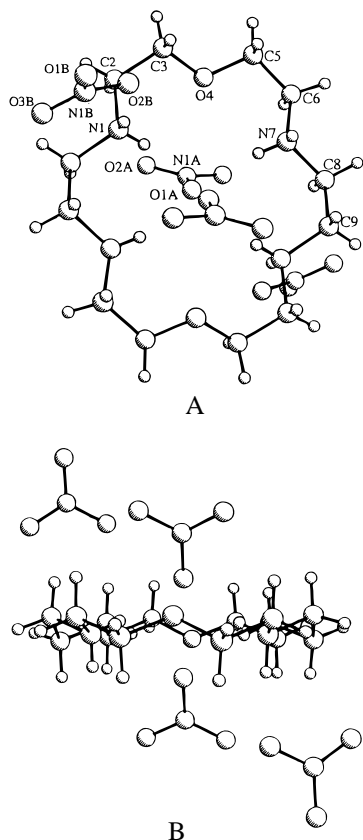(31) Olsen, L. R.; Reed, G. H. *Arch. Biochem. Biophys.* **1993**, *304*, 242−247.

Figure 3. Overhead (A) and side (B) views of $[18]N_4O_2$, **2**·$4NO_3$.

the critical dependence of the catalytic rates of dephosphorylation on the size of the macrocyclic cavity, i.e., a snug fit of receptor and substrate is required for maximum catalytic activity. Hence, large macrocycles are too flexible to form a tight wrap around the nitrate, while 18-membered rings are too small.

There have been a number of reports of crystal structures of macrocyclic complexes with anions although structures with oxoanions are limited. In many cases of anion complexation in general, the anion is outside of the macrocyclic cavity. This is the case for the nitrate complexes of the totally aza 18-membered macrocycle, 1,4,7,10,13,16-hexaazacyclooctadecane $[18]N_6$, including both the tetra(hydrogen nitrate) dihydrochloride[32] and the di(hydrogen nitrate) dihydrochloride,[33] the 24-membered 1,4,7,10,13,16,19,21-octaazacyclotetracosane, $[24]$-N_8,[34] and the nitrate salt of 16-pyridinium crown-4.[35] Hence, the structure of **1**·$4HNO_3$ is somewhat unique in the manner in which the macrocycle envelops the nitrate ion.

Structure of 2·4HNO₃. The crystallographic data for the nitrate complex of the smaller 18-membered analog in its tetraprotonated form, **2**·$4HNO_3$, lends further support to the theory that small ring systems are not good catalysts because their limited size hinders access to the substrates (Figure 3). The macrocyclic ring is no longer boat-shaped but "flat" with essentially a C_{2h} conformation, which is apparently a very stable form as evidenced by the MD simulations, *vide infra*. Although two of the nitrates (A) related by the inversion center appear poised to enter the cavity, the size of the 18-membered ring evidently is prohibitive for inclusion of the anion. All N_{H_2}-

CCO, $N_{H_2}CCN_{H_2}$ and $OCCN_{H_2}$ dihedrals are in the *gauche* conformation, while the others are all *trans*. The structure is somewhat reminiscent of the nitrate complex of a 16-pyrimidinium crown-4 where the nitrate is not in the cavity, but wedged between two pyrimidinium rings.[35] We have also recently isolated and structurally characterized crystals of **2**·4HBr. While the structure is no isomorphous, the positioning of the bromides and the conformation of the macrocycle are essentially identical to that observed for **2**·$4HNO_3$.[36]

The distances between "opposing" macrocyclic nitrogens in **2** are quite short, $N(1)-N(1') = 5.342$ Å and $N(7)-N(7') = 5.368$ Å, compared to the 7.07 Å found for $N(1)-N(1')$ of **1**. The $O(4)-O(4')$ distance is longer, however, at 6.475 Å, unlike the short $O(7)-O(7')$ distance of 3.549 Å in **1**. Given the differences in the size of the macrocyclic cavities, a nucleophilic mechanism for nucleotide dephosphorylation, as in Scheme 1, may not be favored for **2**.

Hydrogen-bonding interactions between $[18]N_4O_2$ and the nitrates are quite strong, especially for nitrate B, which interacts with two macrocycles: $O(2B)-H(1B) = 1.87(4)$ Å and $O(1B)-H(7A)$ of a neighboring macrocycle $= 1.98(3)$ Å.

Molecular Dynamics Simulations. (A) Conformational analysis of the macrocyclic motion of 1·4H⁺. Molecular dynamics simulations for **1** during the first 120 ps indicated very little conformational change from the original X-ray conformation, which indicates that the conformation in the crystal is a stable one in solution. The first conformational transition occurred at 23.3 ps, when one of the $OCCN_{H_2}$ dihedral angles switched from a "g+" to a "g−" conformation. For the next 3 ps the CCOC, COCC, and $CCN_{H_2}C$ dihedrals flipped back and forth between "t" and "g+" conformations and finally returned to the initial conformation. During this time, however, the initial macrocyclic conformation was the dominant one. The coordinates of the macrocycle with four nitrates were averaged for the first 120 ps and are pictured in Figure 4A. During the next 80 ps, the macrocycle showed greater flexibility and underwent a number of conformational transitions. The main conformations which were observed during this period were conformations with "g−" of one of the $CN_{H_2}CC$ dihedrals and with "g−" of the neighboring $N_{H_2}CCO$ dihedral instead of "t" and "g+", respectively, in the initial structure (Figure 4B). The main feature of conformations observed from 200 to 300 ps is that four adjacent dihedrals $CN_{H_2}CC$, $N_{H_2}CCNH$, $CCN_{H}C$, and $CN_{H}CC$ were all in *trans* conformations (Figure 4C). During the next 100 ps four other adjacent dihedrals became *trans* as shown by the average structure from 300 to 400 ps (Figure 4D). As will be seen in the discussion on the influence of hydration *vide infra*, this opening of the macrocycle can be directly attributed to hydration effects. The high population of the original conformation during the first 120 ps could be the result of system preparation and that conformation did not appear after the initial 150 ps.

A number of the conformations of the quadruply-protonated macrocycle are nonunique due to the fact that the folded molecule may have up to C_{2v} symmetry, in which case each dihedral is transformed to three others by symmetry operations. The number of times when $CN_{H}CC$, $N_{H}CCN_{H_2}$, $CCN_{H_2}C$, $CN_{H_2}CC$, $N_{H_2}CCO$, and CCOC dihedrals were observed in particular conformations are shown in Figure 5. While the number of unique conformations found during the simulation was 130, the most frequently found conformations are shown in Table 9, with the most frequently occurring being the initial structure (1205 times, mostly during the first 120 ps). Conformational analysis of the simulation shows that during the

(32) Margulis, T. N.; Zompa, L. J. *Acta Crystallogr., Sect. B* **1981**, *B37*, 1426−1428.

(33) Cullinane, J.; Gelb, R. I.; Margulis, T. N.; Zompa, L. J. *J. Am. Chem. Soc.* **1982**, *104*, 3045−3053.

(34) Bianchi, A. Private communication.

(35) Cramer, R. E.; Fermin, V.; Kuwabara, E.; Kirkup, R.; Selman, M.; Aoki, K.; Adeyemo, A.; Yamazaki, H. *J. Am. Chem. Soc.* **1991**, *113*, 7033−7034.
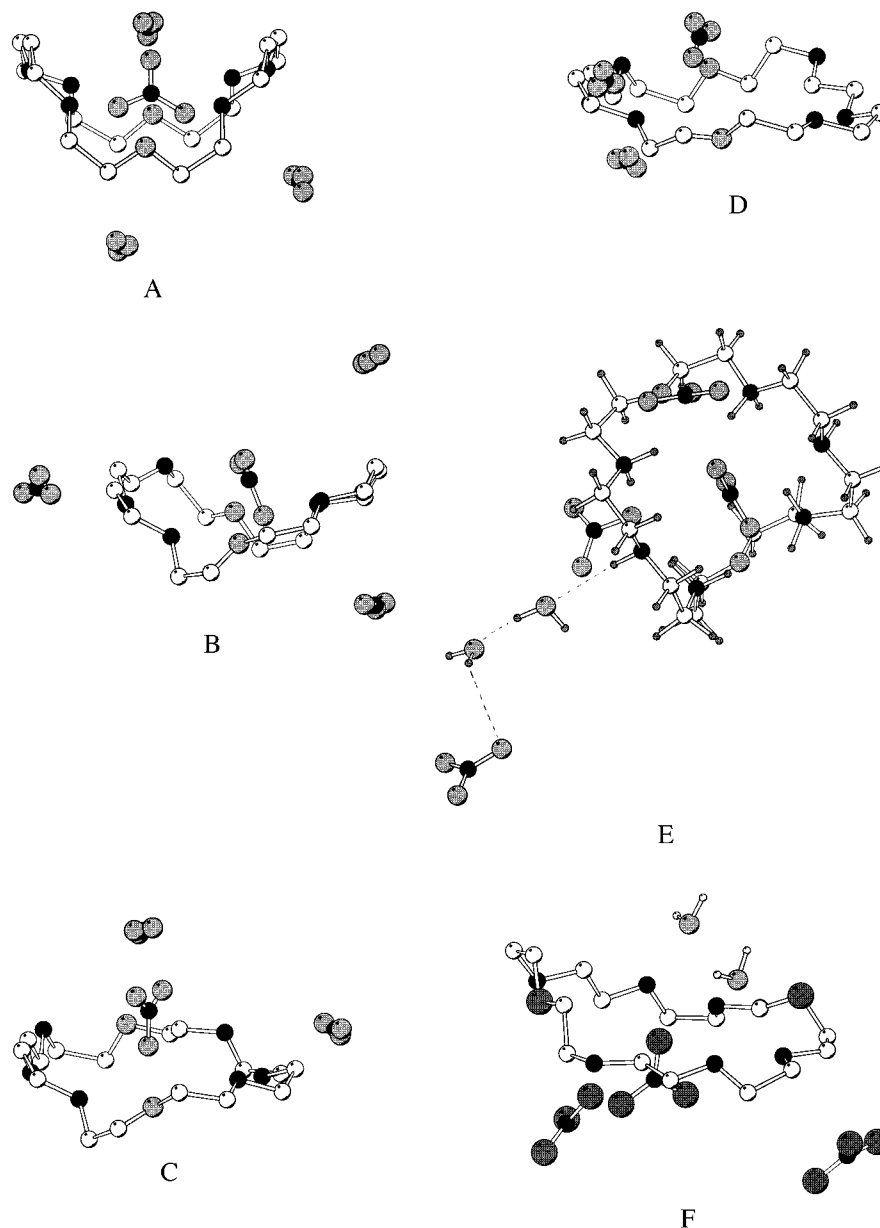
(36) Unpublished results.

Figure 4. Average structures from snapshots of coordinates for $[24]N_6O_2$ (**1·4HNO₃**) over selected time sequences of the simulation: (A) 1200 snapshots during the first 120 ps; (B) 800 snapshots from 120 to 200 ps; (C) 1000 snapshots from 200 to 300 ps; (D) 1000 snapshots from 300 to 400 ps; (E) snapshot at 120 ps showing far ion pair relationship between a nitrate and **1**; (F) final snapshot with two water molecules inside the 4 Å sphere around the center of mass.

time of simulation the macrocycle underwent a number of transitions although only a few highly stable conformations were found. The existence of such stable conformations may be explained by a "locking" effect of the central nitrate, which significantly restricts the number of possible conformations by its incorporation within the macrocyclic cavity.

(B) Analysis of the Mutual Motion of 1·4H⁺ and Four Nitrates. In order to analyze the mutual motion of the macrocycle and nitrates, the distances between the nitrogen atoms of the nitrates and center of mass of the macrocycle were calculated during the entire time of the simulation. The first nitrate, which was initially placed in the center of the macrocycle, remained there throughout the simulation. The major conformational transitions for the macrocycle are easily detectable in Figure 6, which shows the distance between the nitrogens of each nitrate and the center of mass of the macrocycle. The average position of the central nitrate (lowest curve) during the first 120 ps was parallel to a line connecting the two uncharged amino groups, and the nitrate remained at a distance of 0.5 Å

from the center of mass of the macrocycle. This means that the nitrate rotated by 90° from its original position around the axis perpendicular to the macrocyclic ring. After this initial motion it would appear that the barrier to further rotation was somewhat high, since the nitrate did not rotate freely back and forth within the macrocycle during that time period.

The first major transition of the macrocycle occurred at 120 ps, when the distance of the central nitrogen to the center of mass approached 1.5 Å. At that time the nitrate rotated back to its original orientation perpendicular to a line connecting the two uncharged amino groups.

Two additional transitions occurred at 200 and 300 ps, at which times the central nitrate remained at positions of 2–2.5 Å from the center of mass of the macrocycle. Despite the seemingly large distances from the center, the nitrate still remained essentially in the cavity (Figure 4C,D), and these numbers only reflect the fact that the macrocycle lost its symmetrical shape during the course of the simulations. The fact that the nitrate remains topologically inside the cavity

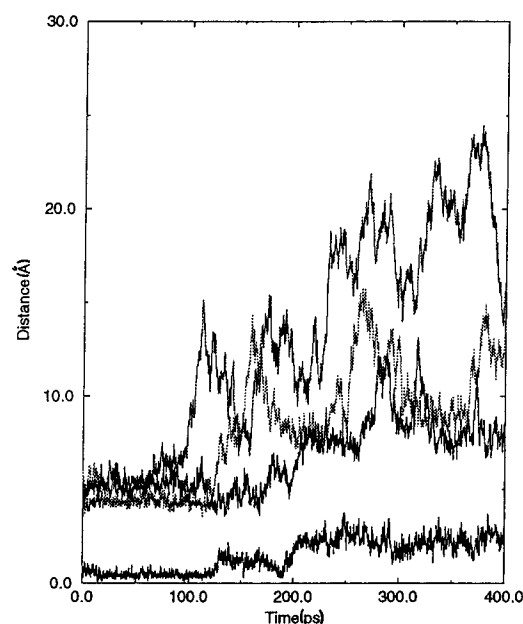**Table 9.** Most Frequently Observed Conformations and Number of Times Observed for $[24]N_6O_2 \cdot 4HNO_3$ (**1**$\cdot$4HNO₃)

																								#
t	g+	t	t	g+	t	t	g-	t	t	g-	t	t	g+	t	t	g+	t	t	g-	t	t	g-	t	1205
t	g+	t	g-	g-	t	t	g+	t	t	g-	t	t	t	t	g-	t	t	t	g-	g-	t	t	t	697
t	g+	t	g-	g-	t	t	g+	t	t	g-	t	t	g+	t	g-	t	g-	t	g-	g-	t	t	t	321
t	g+	t	g-	g-	t	g+	g+	t	t	g-	t	t	g+	t	g-	t	g-	t	g-	g-	t	t	t	171
t	g+	t	t	g-	t	t	g+	t	t	g-	t	t	t	t	g-	t	t	t	g-	g-	t	t	t	152
t	g+	t	g-	g-	t	t	g+	t	t	g-	t	t	g+	t	t	g+	t	t	g-	g-	t	t	t	134
t	g+	t	g-	g-	t	g+	g+	t	t	g-	t	t	g+	t	t	g+	g+	t	g-	g-	t	g-	t	131
t	g+	t	g-	g-	t	t	g+	t	t	g-	t	t	g+	t	g-	t	t	g-	g-	t	t	t		92
t	g+	t	t	t	g-	g-	g+	t	t	g-	t	t	t	t	g-	t	t	t	g-	g-	t	t	t	84
t	g+	t	g-	g-	t	t	g+	t	t	g-	g-	t	g+	t	g-	t	g-	t	g-	g-	t	t	t	57
t	g+	t	g-	g-	t	t	g+	t	t	g-	t	t	g+	t	g-	g-	g-	t	g-	g-	t	t	t	56
t	g+	t	g-	g-	t	t	g-	t	t	g-	t	t	g+	t	t	g+	t	t	g-	g-	t	g-	t	50
g-	g-	g-	g-	g-	t	t	g+	t	t	g-	t	t	t	t	g-	t	t	t	g-	g-	t	t	t	54
t	g+	t	g-	g-	t	g+	g+	t	t	g-	t	t	t	t	g-	t	t	t	g-	g-	t	t	t	54
t	g+	t	t	t	g-	t	g+	t	t	g-	t	t	t	t	g-	t	t	t	g-	g-	t	t	t	53
t	g+	t	g-	g-	t	t	g-	t	t	g-	t	t	g+	t	t	g+	g+	t	g-	g-	t	g-	t	49
t	g+	t	g-	g-	t	t	g+	t	t	g-	t	t	g+	t	g-	g-	t	t	g-	g-	t	t	t	41
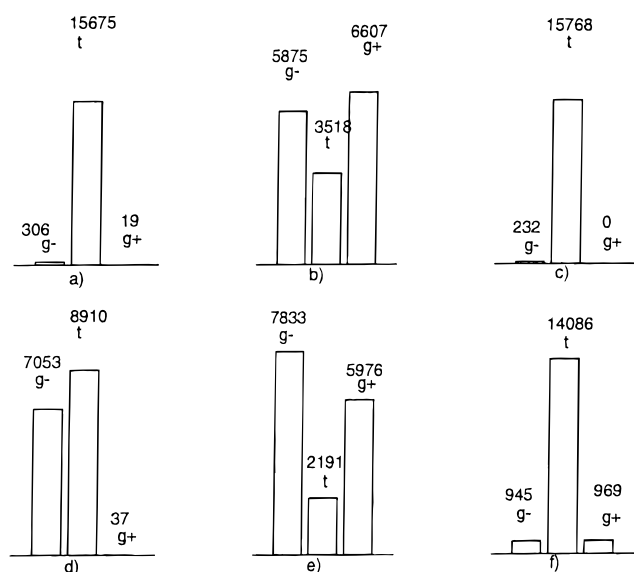
Figure 5. The number of times when dihedrals of $[24]N_6O_2$, **1**$\cdot$4HNO₃ (a) CNHCC, (b) $N_HCCN_{H_2}$, (c) $CCN_{H_2}C$, (d) $CN_{H_2}CC$, (e) $N_{H_2}CCO$, and (f) CCOC were observed at g−, t, or g+ conformations. In each case all symmetry-related dihedrals are taken into account.

Bar chart values:
- a) 306 g-, 15675 t, 19 g+
- b) 5875 g-, 3518 t, 6607 g+
- c) 232 g-, 15768 t, 0 g+
- d) 7053 g-, 8910 t, 37 g+
- e) 7833 g-, 2191 t, 5976 g+
- f) 945 g-, 14086 t, 969 g+

Figure 6. The distance between the nitrogen of all nitrates and the center of mass of the $[24]N_6O_2$, **1**, as a function of time. The lowest line is the nitrate inside the macrocyclic cavity.

created by the macrocycle during the entire length of the simulations, however, is quite remarkable. It indicates that the host−guest interactions between the macrocycle and the nitrate are strong not only in the solid state but also in solution.

The three nitrates moving outside the macrocyclic cavity showed significantly different patterns of movement than the central nitrate. During the first 100 ps of the simulation all of the nitrates remained at distances of 5−6 Å from the center of mass (Figure 6). Since this is the closest distance of approach of the external nitrates, this could be called the "first anionic shell". At 100 ps one of the nitrates left this first shell and remained at a distance between 6 and 15 Å from the macrocycle, finally leaving the area at 220 ps. The remaining two nitrates showed mutually correlated oscillatory motion between similar positions at 6−15 Å from the center of mass of the macrocycle. These positions correspond to 0.5−9 Å from the actual "surface" of the macrocycle.

At these distances several types of ion pairs may be identified: contact ion pairs, involving macrocyclic contact without solvent separation; close ion pairs, with one solvent molecule between the positive and negative ions; and far ion pairs, with two solvent molecules between the opposing ions. The pair distribution functions for the nitrogens of the nitrates and the center of mass of the macrocycle for the three nitrates outside of the ring are shown in Figures 7−9. In the case of the nitrates which remained close to the macrocycle during the simulations and labeled for bookkeeping purposes as 2 and 3, the pair distribution functions show two peaks in each case at approximately 4 and 8 Å. These can be attributed to contact- and one-solvent-separated pairs (Figures 7 and 8) and are associated with the two nitrates which were undergoing bound oscillatory motion around the macrocycle (Figure 6). There are three distinct peaks for the pair distribution function of the fourth nitrate, which resided at a farther distance from the macrocycle for longer periods (Figure 9). The first two peaks at about 5 and 6 Å correspond to the different orientations of the contact ion pair, and the third at 11 Å corresponds to the two-solvent-separated ion pair. The absence of the close ion pair for this nitrate is possibly due to the fact that this nitrate was found at distances between 8 and 9 Å for only short periods (Figure 6). Likewise, because the other two nitrates outside of
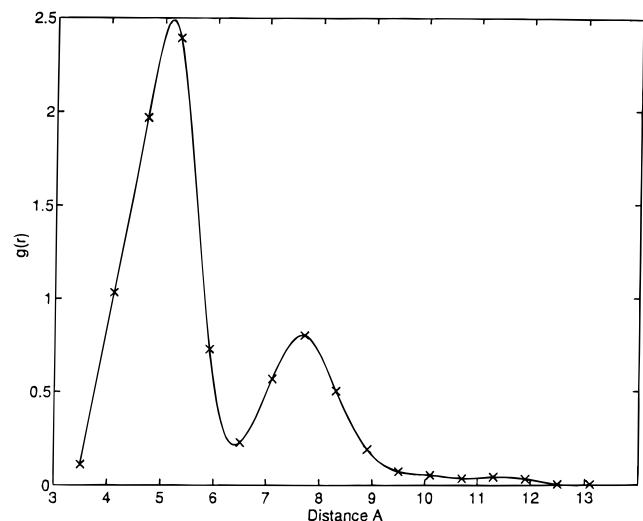
Figure 7. The pair distribution function for the nitrogen of the second nitrate as related to the center of mass of [24]N$_6$O$_2$, **1**.
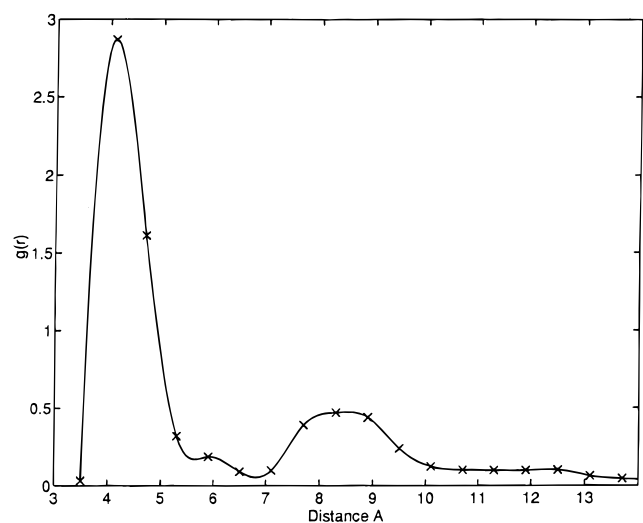

Figure 8. The pair distribution function for the nitrogen of the third nitrate as related to the center of mass of [24]N$_6$O$_2$, **1**.
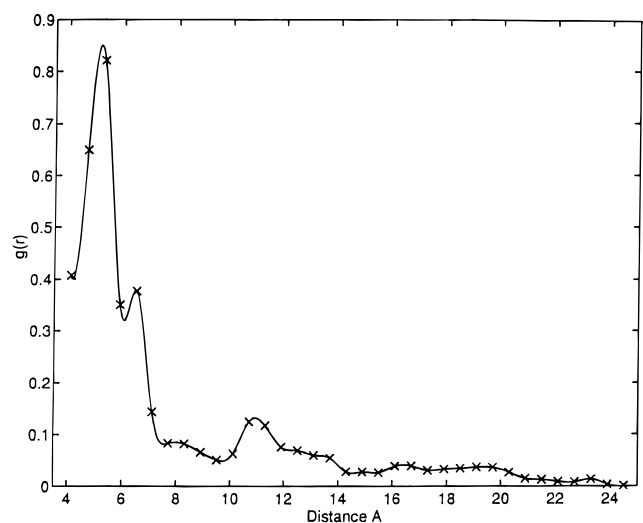

Figure 9. The pair distribution function for the nitrogen of the fourth nitrate as related to the center of mass of [24]N$_6$O$_2$, **1**.

the macrocyclic cavity remained closer to the macrocycle, the role of far ion pairs for these two nitrates was not observed. A snapshot of the water relay for the far ion pair situation is shown in Figure 4E.

The concept of far ion pairs is well-documented from the statistical mechanics of pure liquids,[37] but to our knowledge, it has not been reported from molecular dynamics or Monte Carlo simulations. It is highly probable that the four negatively charged nitrate ions in conjunction with the multiple positive charges on the macrocycle are responsible for the stronger polarization of water dipoles and the observation of far ion pairs. Thus, electrostatic relay interactions exist through the water molecules, which are responsible for linking the far ion pairs to the macrocycle at distances greater than the direct nonbonded interaction cutoff. This finding may shed light on understanding the reaction mechanisms occurring in multicharged systems in aqueous solution as, for example, in reactions in which an initial step involves the formation of an outer sphere complex.

(C) Analysis of the Water Structure of 1·4HNO$_3$. As previously observed, the structure of the solvent greatly affects the conformational and structural preferences of the macrocycle and binding modes of the ligands.[13–18] For example, it was reported by Kollman and Bayly[16a] that the secondary affinity of an 8-subunit(anisol)-cavitand toward sodium ion resulted from the incorporation of two water molecules into the cavity of the macrocycle and their ability to hydrogen bond with the surroundings. Studies of the capture of chloride anion by a tetraprotonated macrotricyclic cryptand also indicated the importance of hydration and dehydration processes for the height of the energy barrier between two binding sites, in and outside of the cavity of the macrocycle.[38] In earlier MD studies of **1**·6HCl a significant change in the conformation of the macrocycle upon simulation in a water solution was observed, although the short time of the simulation (10 ps) did not allow for definitive conclusions.[18]

In the structure of **1**·4HNO$_3$ the data indicated that the hydrogens of all of the NH$_2^+$ groups pointed inside the cavity of the macrocycle, and it was anticipated that some of them would undergo conformational transitions to turn toward the bulk solvent. This transition occurred after 200 ps of simulations (Figure 4C,D) as part of the hydration process, at which time the macrocycle lost its symmetrical shape and flattened significantly. The numbers of water molecules around the center of mass of the macrocycle (calculated as an integral of $g(r)$) averaged over the four periods of the simulation were calculated. There were no water molecules inside the cavity of the macrocycle in the initial stage (0–120 ps) of the simulation, and only nine water molecules surrounded the macrocycle in a 6.0 Å shell near its center of mass. Upon the opening of the macrocyclic cavity, the number of water molecules in the 6.0 Å coordination shell near the central nitrate nearly doubled, significantly increasing the solute–water attractive interactions and strongly favoring the process of flattening. Almost identical patterns for numbers of water molecules between 200–300 and 300–400 ps indicate that the process of hydration of the macrocycle was essentially complete after 200 ps. While the cavity of the macrocycle in the boat form was well-suited for the single nitrate ion, the flattening of the macrocycle allowed for the incorporation of two additional water molecules (Figure 4F).

An analysis of the process of hydration of the three "outside" nitrates indicated much better solvation at the initial stages of the simulation although their complete hydration also required over 200 ps. Including all of the species involved, it was observed that the relaxation time for the water network around

(37) Chandler, D. In *Introduction to Modern Statistical Mechanics*; Oxford University Press: New York, 1987.
(38) (a) Owenson, B.; MacElroy, R. D.; Pohorille, A. *J. Am. Chem. Soc.* **1988**, *110*, 6992–7000. (b) Owenson, B.; MacElroy, R. D.; Pohorill, A. *THEOCHEM* **1988**, *179*, 467–484.

Table 10. Most Frequently Observed Conformations and Number of Times Observed for $[18]N_4O_2\cdot 4HNO_3$ ($2\cdot 4HNO_3$)

Conformations																		Time(ps)	#	Symm.
t	g+	t	t	g−	t	t	g+	t	g+	g+	t	t	g+	t	t	g−	t	1.0	47	C_1
t	g+	t	t	g−	t	t	g+	t	g+	g+	t	t	g−	g−	t	g−	t	4.8	36	C_s
t	g+	t	t	g−	t	t	g+	t	g+	g+	t	t	g−	g−	t	t	t	5.1	21	C_1
g−	g−	t	t	g+	g+	t	t	t	g+	g+	t	t	g−	g−	t	g−	t	14.4	17	C_2
g−	g−	t	t	g+	g+	t	t	t	g+	g+	t	t	g−	g−	t	t	t	16.4	801	C_{2h}
g−	g−	t	t	g−	g+	t	t	t	g+	g+	t	t	g−	g−	t	t	t	24.9	12	C_1
g−	g−	t	t	g−	t	t	t	t	g+	g+	t	t	g−	g−	t	t	t	25.0	14	C_1
g−	g−	t	t	g+	g+	t	t	t	g+	g+	t	t	g−	g+	t	t	t	73.0	127	C_1
g−	g−	t	t	g−	g+	t	t	t	g+	g+	t	t	g−	g+	t	t	t	75.9	17	C_1
g−	g−	t	t	g−	t	t	t	t	g+	g+	t	t	g−	g+	t	t	t	76.6	12	C_1
t	g+	t	t	g−	g+	t	t	t	g+	g+	t	t	g−	g+	t	t	t	77.4	12	C_1
t	g+	t	t	g−	t	t	t	t	g+	g+	t	t	g−	g+	t	t	t	77.6	17	C_1
t	g+	t	t	g−	g+	t	t	t	g+	g+	t	t	g−	g+	t	t	g+	77.8	112	C_1
t	g+	t	g−	g−	g+	t	t	t	g+	g+	t	t	g−	g+	t	t	g+	78.1	24	C_1
t	g+	t	t	g−	g+	t	t	t	g+	g+	g+	t	g−	g+	t	t	g+	78.7	19	C_1
t	g+	t	t	g−	t	t	t	t	g+	g+	t	t	g−	g+	t	t	g+	81.8	27	C_1
t	g+	t	g−	g−	t	t	t	t	g+	g+	t	t	g−	g+	t	t	g+	87.9	12	C_1
t	g+	t	t	g−	t	t	t	t	t	g−	t	t	g−	g+	t	t	t	93.3	11	C_1
t	g+	t	t	g+	g+	t	t	t	g+	g+	t	t	g−	g+	t	t	g+	94.8	104	C_1
t	g+	t	t	g+	g+	t	t	t	t	g−	t	t	g−	g+	t	t	g+	100.9	110	C_1
t	g+	t	t	g+	g+	t	t	t	t	g−	t	t	g−	t	t	t	g+	103.9	40	C_1
g−	g−	t	t	g+	g+	t	t	t	t	g−	t	t	g−	g+	t	t	g+	105.7	66	C_1
g−	g−	t	t	g+	g+	t	t	t	g+	g+	t	t	g−	g+	t	t	g+	110.3	59	C_1
g−	g−	t	t	g+	g+	t	t	t	g+	g−	t	t	g−	g+	t	t	g+	114.9	23	C_1
g−	g−	t	t	g+	g+	t	t	t	g+	g+	g+	t	g−	g+	t	t	t	137.6	14	C_1

the charged species can be up to 200 ps, which should be taken into consideration when examining equilibrium in aqueous solutions of charged molecules.

It is well-established that the overall energy of the process of desolvation includes solute−solute, solute−water, and water−water interaction terms. The strongly attractive interactions between the central nitrate and the macrocycle in the initial structure results in the favorable boat conformation in the solid state. In aqueous solution, however, this conformation does not allow the best hydration of the macrocycle and the central nitrate. It can be postulated, therefore, that the enhancement of the solute−water interaction term is a driving force for transitions to more "opened", flattened conformations along with the inclusion of two water molecules within the macrocyclic sphere. Nonetheless, the fact that the central nitrate remains in the cavity of even the flattened macrocycle strongly suggests that this macrocycle is an excellent receptor for nitrate ion.

(D) Conformational Analysis of 2·4HNO₃. Due to the fact that the macrocycle was considerably more planar in the crystal structure, it was "better-prepared" for solvation. During the simulation, all of the observed conformations were also flat and close to the initial structure. The macrocycle lost its original C_{2h} conformation during the heating and equilibration phases of the simulation, but regained it again at 16.4 ps into the dynamics phase. This was the most frequently observed conformation (801 times, Table 10). The related C_2 and C_s conformations were observed 17 and 36 times, respectively. None of the other conformations which were derived from the C_{2h} by a few dihedral transitions possessed any element of symmetry. The number of unique conformations detected throughout the simulation was 120.

In every conformation all of the four $N_{H_2}CCO$ dihedrals were in the g+ or g− conformation, which allowed for strong hydrogen bonding between polar hydrogens of NH_2^+ groups and the ether oxygen. The stability of the C_{2h} conformation and its derivatives may be attributed to hydrogen bonding along with the possibility of strong hydration of an "open" structure
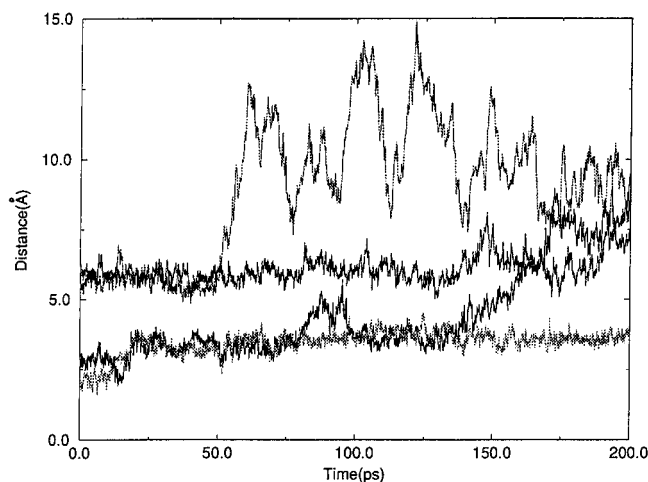

Figure 10. The distance between the nitrogen of all nitrates and the center of mass of $[18]N_4O_2$, $2\cdot 4HNO_3$.

of the macrocycle. At the end of the simulation (200 ps) the macrocycle was observed almost only in the C_{2h} conformation. This suggests that this conformation is stable not only in the solid state but also in solution, contrary to what was observed for $1\cdot 4HNO_3$, which showed significantly different conformational preferences in solution than in the solid state.

(E) Analysis of the Mutual Motion of 2·4H⁺ and Four Nitrates. As in the case of the simulation of **1**, the distances between the center of mass of the macrocycle and the nitrogens of the nitrates were monitored throughout the simulation (Figure 10). Initially two types of nitrates existed around the macrocycle: the first and third nitrates remained bound from above and below the plane of the macrocycle to the pairs of NH_2^+ groups at a distance of about 3 Å. The second and fourth nitrates moved freely around the macrocycle, forming contact ion pairs at a distance of about 6 Å. The two modes of binding of the nitrates are clearly shown in Figure 11A, a snapshot of the system at 20 ps. After 50 ps the fourth nitrate left the nearest
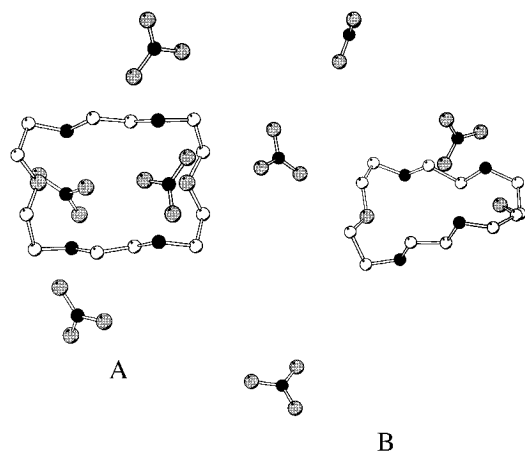
Figure 11. Snapshot of [18]N$_4$O$_2$, **2**·4HNO$_3$: (A) at 20 ps; (B) at 180 ps.

shell around the macrocycle and formed solvent-separated ion pairs between 7 and 15 Å from the center of mass of the macrocycle. Hence, the stability of far ion pairs was confirmed once again in this simulation.

The system with the first and third nitrates bound from above and below the plane of the molecule existed until 150 ps, at which time the third nitrate left the cavity. The first nitrate remained asymmetrically bound to the pair of NH$_2^+$ groups during the entire simulation (Figure 11B). Between 150 and 200 ps, the other three nitrates were coordinated to the macrocycle through one bridging water molecule in each case, therefore forming one-solvent-separated ion pairs. Since the two nitrates were simultaneously bound to the cavity of the macrocycle for 150 ps, **2**·4HNO$_3$ may also be regarded as a receptor for nitrate ion.

(F) Analysis of the Water Structure of 2·4HNO$_3$. Due to the "open" nature of the C_{2h} conformation of **2**·4HNO$_3$, the relaxation of the hydration shell was expected to occur more rapidly than 200 ps. The number of water molecules inside the sphere around the center of mass of the macrocycle was monitored throughout the simulation. At the beginning of the dynamics simulation, the macrocycle was surrounded by 9 or 10 water molecules inside a sphere of 6 Å radius. The water

network around the macrocycle was completely equilibrated after 50 ps for the conformation of the macrocycle with two bound nitrates, and included 11 or 12 water molecules. After dissociation of the third nitrate, one side of the macrocycle became more open for interaction with water molecules and three additional water molecules entered the 6 Å sphere. Similar situations were observed for the remaining nitrates, which reached equilibration on a faster time scale (ca. 50 ps) compared to **1**.

Hence, relaxation of a water network around complex charged species can take a fairly long time (200 ps for **1** and 50 ps for **2**). These equilibrations are not only a function of charge but also of the possibility of conformational and structural transitions within a charged system. The analysis of the water structure is thus a powerful tool for understanding binding abilities of different receptors toward a given anion and can provide significant insight into the mechanisms of conformational transitions occurring during a multitude of reactions, including the phosphoryl transfer reactions which initially prompted this study.

Supporting Information Available: Complete crystal data, bond distances and angles, atomic coordinates, and thermal parameters of **1**·4NO$_3$ and **2**·4NO$_3$ (52 pages); structure factors for **1**·4NO$_3$ and **2**·4NO$_3$ (19 pages). This material is contained in many libraries on microfiche, immediately follows this article in the microfilm version of the journal, can be ordered from the ACS, and can be downloaded from the Internet; see any current masthead page for ordering information and Internet access instructions.

JA9500567